AD-770 091

MAGNETIC ANOMALY DETECTION UTILIZING COMPONENT DIFFERENCING TECHNIQUES

Brooks C. Fowler, et al

Texas University

Prepared for:

Office of Naval Research

31 August 1973

Security Classification

AD 770091

DOCUMENT CONTROL DATA - R & D

(Security classification of title, body of abstract and indexing annotation must be entered when the overall report is classified)

1. ORIGINATING ACTIVITY *(Corporate author)*
The University of Texas
Electronics Research Laboratory
Austin, Texas

2a. REPORT SECURITY CLASSIFICATION
Unclassified

2b. GROUP

3. REPORT TITLE
MAGNETIC ANOMALY DETECTION UTILIZING COMPONENT DIFFERENCING TECHNIQUES

4. DESCRIPTIVE NOTES *(Type of report and inclusive dates)*
Final Report

5. AUTHOR(S) *(First name, middle initial, last name)*
Brooks C. Fowler, H. W. Smith and F. X. Bostick, Jr.

6. REPORT DATE	7a. TOTAL NO. OF PAGES	7b. NO. OF REFS
August 31, 1973	~~43~~ 45	18

8a. CONTRACT OR GRANT NO.	9a. ORIGINATOR'S REPORT NUMBER(S)
N00014-67-A-0126-0011 b. PROJECT NO. NR 371-032 c. d.	Final Report 9b. OTHER REPORT NO(S) *(Any other numbers that may be assigned this report)*

10. DISTRIBUTION STATEMENT
Distribution of this document is unlimited.

11. SUPPLEMENTARY NOTES	12. SPONSORING MILITARY ACTIVITY
	Office of Naval Research Electronics Program Office Arlington, Virginia 22217

13. ABSTRACT

A scheme for the detection of the passage of ships and other permeable objects which utilizes stationary component magnetometers is described. The system requires as complete a cancellation of the natural geomagnetic micropulsation noise as is possible in the frequency range from 0.001 to 1 Hz. A simple method for detecting the magnetic anomaly produced by a passing ship is to form the difference between parallel components of the magnetic field variations at each end of a baseline several miles in length. The geomagnetic micropulsation noise tends to cancel, but the target anomaly is more localized and causes each magnetic sensor to operate almost independently for the target detection. However, in many locations the variation in local geology along the baseline introduces a "geology filter" which must be removed by more elaborate measurement and computation.

Results are presented for the detection of ship passage at ranges up to one mile during a series of tests at Port Aransas, Texas in the summer of 1971. In addition the results obtained from a field test program designed to demonstrate the capability of removing the geology effects are included. These tests were conducted near Manor, Texas in the summer of 1972.

DD FORM 1 NOV 65 1473 (PAGE 1) PLATE NO. 21856

S/N 0102-014-6600

1a

Security Classification

Security Classification

14 KEY WORDS	LINK A		LINK B		LINK C	
	ROLE	WT	ROLE	WT	ROLE	WT
Magnetic gradiometer						
Magnetic Anomaly Detection						

ib

DD FORM 1 NOV 68 1473 (BACK)
(PAGE 2)

Security Classification

MAGNETIC ANOMALY DETECTION UTILIZING COMPONENT DIFFERENCING TECHNIQUES

by

Brooks C. Fowler, H. W. Smith,
and F. X. Bostick, Jr.
Department of Electrical Engineering

FINAL REPORT
August 31, 1973

ELECTRICAL GEOPHYSICS RESEARCH LABORATORY

prepared under
Contract N00014-67-A-0126-0011
Office of Naval Research

Electronics Research Center
The University of Texas at Austin
Austin, Texas 78712

IC

TABLE OF CONTENTS

LIST OF FIGURES

LIST OF TABLES

I. INTRODUCTION

The Electrical Geophysics Research Laboratory of The University of Texas at Austin has been developing over the past four years an ultra-sensitive stationary magnetic anomaly detection system. This sytem operates in the micropulsation frequency range from 0.001 to 1 Hz and is capable of detecting the magnetic anomaly produced by the passage of ships or other permeable objects. The term magnetic gradiometer is used to describe this detection system.

Operation of the magnetic gradiometer is based on the following principles. The natural geomagnetic micropulsation fields tend to be relatively uniform in space. In most cases the magnetic fields of an anomaly, such as a passing ship or automobile, are more localized in space than are the micropulsation fields. A simple method for detecting the anomaly is to form the difference between parallel components of the magnetic field variations measured at each end of a baseline. The micropulsation field variations affect the sensors at both ends of the baseline almost equally. They tend to subtract out in the difference trace. The micropulsation field variations are thus nulled in the difference trace. Although the system operates as a gradiometer for nulling the low gradient micropulsation noises, it does not operate as a gradiometer on the target signals. The target anomaly, with its localized field, will affect the field component of the near sensor more than the field component at the other end of the baseline. The relatively large baseline separating the two measuring points causes each magnetic sensor to operate almost independently when sensing a target signal within the detection range. The target anomaly is not nulled by the differencing process.

This simple differencing scheme provides a considerable reduction in the detection system noise to a level below that of the mean micropulsation activity. The result is an improvement in the ratio of anomaly signal to the residual micropulsation noise level in the difference trace.

The detection capabilities of the gradiometer depend upon several parameters of the target itself, none of which are controllable, and the degree to which it is possible to obtain a perfect null in the absense of a target. There are three important factors contributing to the amount of noise power in the null:

1. The micropulsation source wave is not perfectly coherent over the spearation distance.

2. Noise in the measuring and recording equipment.

3. The effect of the local geology on the magnetic field variations.

The first factor is uncontrollable and imposes an ultimate limit on the detection range of the system. It is the puspose of this report to describe the progress which has been made in the reduction of the noise resulting from the last two factors. Results are presented for the magnetic gradiometer detection of ship passage at ranges up to one mile during a series of tests at Port Aransas, Texas, in the summer of 1971. In addition, the results obtained from a field test program designed to demonstrate the capability of removing the geology effects are included. These tests were conducted near Manor, Texas in the summer of 1972.

II. THE MAGNETIC GRADIOMETER

For the magnetic gradiometer detection system the prime objective is the cancellation of the natural micropulsation field as completely as possible between the two measuring points. In regions where the geology is fairly uniform over the separation distance, cancellation may be accomplished by the simple differencing scheme. However, when the geology is more complex the micropulsation source wave will undergo reflections that can cause significant spatial variations. In this case the cancellation (and thus detection performance) will deteriorate due to the local geology effects and a multicomponent system is needed to reduce the micropulsation noise.

A. Local Geology Effects

Micropulsation fields are vector fields for which it is characteristic that the orthogonal components are incoherent to some degree. It can be misleading to consider relationships between only the parallel components at the two measuring sites if there are significant changes in the geology between the sites. A portion of the energy in the measured component is due to the reflected wave. Any inhomogeneities in the geology between the two sites may change the reflected wave at one site both in intensity and direction relative to the other site. Thus any component of the measured micropulsation field at one site may appear to have a measure of incoherence with the respective component at the other end of the baseline due to the geology effects.

These effects are equivalent to a misalignment of the two component sensors even if they are geometrically parallel. Furthermore, the effective misalignment is a variable of frequency since the effect of the inhomogeneous earth is a variable of frequency. As Madden [7] points out, a more involved treatment is necessary when dealing with vector fields, and the full vector relationships must be considered.

B. Geology Filter Model

A simple model for simulating the effects of the local geology upon the measured micropulsation field is given as follows. Consider that the earth acts as a two-input-channel linear filter. The inputs to the filter are the two orthogonal components of the micropulsation source wave, which are assumed to have some degree of independence. The transfer characteristics of the filter are determined by the geology below the measuring site. The three orthogonal components of the reflected wave are the outputs of the filter. Each horizontal component of the measured micropulsation field is composed of an incident and a reflected wave. This is represented in the model by the sum of an input and an output of the filter. The vertical component of the measured field is assumed to be strictly a secondary field. The model is shown in Figure (2-1).

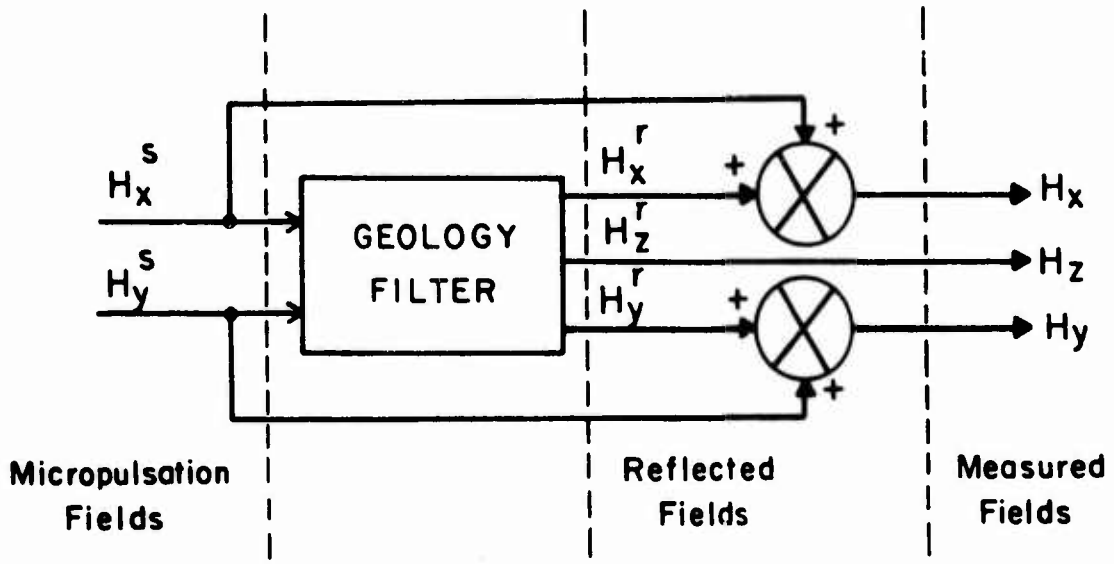

Figure 2-1. Geology Filter Model

The model shown in Figure 2-1 represents the effect of the geology below one of the measuring sites. At the other end of the baseline the geology and thus the geology filter may be considerably different. In this model it is assumed that there exists an equivalent transfer function which relates the transfer function of the filter for one site to the transfer function of the filter for the site at the other end of the baseline. If the equivalent transfer function is known or can be estimated, it may be applied to the measured components at one site. The result can then be differenced with the components at the other site to null the micropulsation field.

The above model is equivalent to assuming that there exists a linear relationship between the three components of the measured micropulsation field at one site, called the base site, and any single component of the measured field at the other site, called the remote site,

$$H_F(f) = H_R(f) - A(f)H_x(f) - B(f)H_y(f) - C(f)H_z(f) \qquad (2\text{-}1)$$

In Equation (2-1), $H_R(f)$ is the Fourier transform, at frequency f, of the output of a single component sensor at the remote site; $H_x(f)$, $H_y(f)$, and $H_z(f)$ are the Fourier transforms of the three orthogonal components at the base site. The terms A(f), B(f), and C(f) represent the linear relationship between the remote and base sites and are called the geology filter.

The residual term $H_F(f)$ is a noise term and is identified as the filtered null. Equation (2-1) is called a cancellation process since it is an attempt to completely null the micropulsation fields observed at the two sites. In the absence of a target signal, a non zero filtered null may be attributed to

1. Measurement noise,
2. Imperfect estimation of the geology filter,
3. Spatial incoherency or gradients in the source wave.

When the target signal or anomaly occurs, it will again perturb the field at the near sensor(s) and will not be present to any degree at the far sensor(s).

The anomaly signal is thus in the filtered null output with the residual micropulsation noise reduced due to application of the geology filter.

III. ESTIMATION OF THE GEOLOGY FILTER

A. Estimation

Since the geology parameters are not known precisely for a particular gradiometer site, the geology filter must be estimated from micropulsation data measured at that site. Once the data is acquired from the site in question, it may be digitized and the estimation performed using a digital computer. It is possible to estimate the geology filter weights in the time domain or to estimate the geology transfer function in the frequency domain. In either case, one may invoke the minimum mean-square error criterion. As implemented, the two approaches are not exactly equivalent; the major differences are the spectral windows involved and the computational effort required. Estimation in the frequency domain is preferred here.

The discrete Fourier transform is computed for each of the three orthogonal components of the measured micropulsation field at the base site and also the single component at the remote site. These transforms will again be denoted by $H_x(f)$, $H_y(f)$, $H_z(f)$, and $H_R(f)$, respectively. Once the transforms have been obtained, the geology filter, $A(f)$, $B(f)$, and $C(f)$ can be estimated in the mean square sense by defining an error function,

$$E(f) = H_R(f) - A(f)H_x(f) - B(f)H_y(f) - C(f)H_z(f). \qquad (3\text{-}1)$$

The correspondence of the error function and the geology filter model, equation (2-1), is noted. Recall, however, that the field components were obtained from physical measurements and the transforms will contain measurement noise.

The mean-square error is

$$\begin{aligned} \Phi &= \sum_{i=1}^{n} E_i(f)\, E_i^*(f) \\ &= \sum_{i=1}^{n} [H_{Ri}(f) - A(f)\, H_{xi}(f) - B(f)\, H_{yi}(f) - C(f)\, H_{zi}(f)] \\ &\quad [H_{Ri}^*(f) - H_{xi}^*(f)\, A^*(f) - H_{yi}^*(f)\, B^*(f) - H_{zi}^*(f)\, C^*(f)] \end{aligned} \qquad (3\text{-}2)$$

where there are n measurements of the field components at the discrete frequency f. The superscript asterisk indicates the complex conjugate. Estimation of the geology filter is made by minimizing the mean-square error with respect to each of the real and imaginary parts of the filter. One finds the values of A(f), B(f), and C(f) that minimize Ψ by setting

$$\frac{\partial \Psi}{\partial \mathrm{Re}\{A(f)\}} = \frac{\partial \Psi}{\partial \mathrm{Im}\{A(f)\}} = 0 \qquad (3\text{-}3a)$$

$$\frac{\partial \Psi}{\partial \mathrm{Re}\{B(f)\}} = \frac{\partial \Psi}{\partial \mathrm{Im}\{B(f)\}} = 0 \qquad (3\text{-}3b)$$

$$\frac{\partial \Psi}{\partial \mathrm{Re}\{C(f)\}} = \frac{\partial \Psi}{\partial \mathrm{Im}\{C(f)\}} = 0 \qquad (3\text{-}3c)$$

where Re{ } denotes the real part and Im{ } denotes the imaginary part. The following set of equations follow from the above,

$$\sum_{i=1}^{n} H_{Ri}H_{xi}^{*} = A\sum_{i=1}^{n} H_{xi}H_{xi}^{*} + B\sum_{i=1}^{n} H_{yi}H_{xi}^{*} + C\sum_{i=1}^{n} H_{zi}H_{xi}^{*} \qquad (3\text{-}4a)$$

$$\sum_{i=1}^{n} H_{Ri}H_{yi}^{*} = A\sum_{i=1}^{n} H_{xi}H_{yi}^{*} + B\sum_{i=1}^{n} H_{yi}H_{yi}^{*} + C\sum_{i=1}^{n} H_{zi}H_{yi}^{*} \qquad (3\text{-}4b)$$

$$\sum_{i=1}^{n} H_{Ri}H_{zi}^{*} = A\sum_{i=1}^{n} H_{xi}H_{zi}^{*} + B\sum_{i=1}^{n} H_{yi}H_{zi}^{*} + C\sum_{i=1}^{n} H_{zi}H_{zi}^{*} \qquad (3\text{-}4c)$$

where the notation for dependence on frequency has been dropped. Notice that the summations represent auto- and cross-power density spectra. The solution to the above set of equations is, in matrix form,

$$[A\ B\ C] = [\overline{H_R H_x^*}\ \overline{H_R H_y^*}\ \overline{H_R H_z^*}] \begin{bmatrix} \overline{H_x H_x^*} & \overline{H_x H_y^*} & \overline{H_x H_z^*} \\ \overline{H_y H_x^*} & \overline{H_y H_y^*} & \overline{H_y H_z^*} \\ \overline{H_z H_x^*} & \overline{H_z H_y^*} & \overline{H_z H_z^*} \end{bmatrix}^{-1} \quad (3\text{-}5)$$

where A, B, and C are estimates of the true geology filter and the bar indicates the averaging process. Estimation of the geology filter is reduced to obtaining reliable estimates of the auto- and cross-power spectral densities.

In magnetotelluric analysis, apparent resistivity curves are smooth and regular when they are plotted on log-log scales. Investigators in this area [12, 13] find it natural to employ a logarithmic type of bandiwdth averaging in the estimation of these same spectral densities considered here. Frequency bands are used whose center frequencies are equispaced on a logarithmic scale. This is termed constant Q averaging. The geology filter is an attempt to model geology differences, not the geology itself. However, physical intuition leads one to believe that the geology filter should also be slowly varying with frequency. There are many so-called spectral windows discussed in the literature [1]. It appears that the particular window used is mostly a matter of choice for the application at hand. The constant Q averaging type of spectral window seems a logical choice for this work.

B. Application

For the estimation and subsequent application of the geology filter in the frequency domain, a discussion of the techniques involved is presented here. The discrete Fourier transformation of the digitized data from any one of the four coils may be written as

$$H(f) = \frac{1}{N} \sum_{t=0}^{N-1} h(t)\, e^{-j2\pi ft/N} \quad (3\text{-}6)$$

where the harmonic number index, $f = \{0, 1, 2, \ldots, N-1\}$, and the discrete time index, $t = \{0, 1, 2, \ldots, N-1\}$. There are N sample points in the time series. For the Fast Fourier Transform algorithm, N is chosen as a power of 2, usually 8192 for this work.

If the time series is digitized at intervals of $\Delta t = 6.4$ seconds, the fundamental frequency is

$$f_o = \frac{1}{N\Delta t} \tag{3-7}$$

and the true frequency at any one of the harmonics is obtained by multiplying the harmonic number by the fundamental. The folding or Nyquist frequency is

$$f_N = \frac{1}{2\Delta t} \tag{3-8}$$

Since the time series h(t) is a real-valued function, the real part of H(f) is symmetric about the folding frequency f_N. The imaginary part of H(f) is antisymmetric about the folding frequency.

After the transforms, $H_R(f)$, $H_x(f)$, $H_y(f)$, and $H_z(f)$ are obtained; the raw power spectra, $H_i(f)\ H_j^*(f)$, are computed for each harmonic frequency up to the folding frequency,

where

$$f = \{0, 1, 2, \ldots, \frac{N}{2}\},$$

$$i = \{x, y, z, R\},$$

$$j = \{x, y, z, R\}.$$

The average spectra, $\overline{H_i(f)H_j^*(f)}$, is the result of constant Q averaging. After this type of smoothing, the frequency components of the average spectra are reduced from $\left(\frac{N}{2} + 1\right)$ and are equispaced on a logarithmic scale.

These average spectra are inserted into equation (3-5) for estimation of the geology filter. The resulting estimate is also evenly spaced on a logarithmic scale. Recall from equation (2-1) that the geology filter must be applied to the data to obtain the filtered null $H_F(f)$. Since the data, $H_x(f)$, $H_y(f)$, $H_z(f)$ have frequency components which are linearly spaced, the estimate of the geology filter is interpolated at equal increments in frequency. The interpolation is made using a cubic spline fit [9]. Then the filter can be applied to yield the null. The result can then be inverse transformed to present the filtered null as a time function.

IV. DATA ANALYSIS

A. Data Acquisition

Estimation of the geology filter requires data measured at the site where the magnetic gradiometer is to be used. The data used in the following analysis was obtained with the magnetotelluric instrumentation system developed by the Electrical Geophysics Research Laboratory at The University of Texas at Austin. This system has been discussed in detail by Word [19], Bostick [3], and Hopkins [7]. Only a brief description will be given here.

The system is equipped to measure the three orthogonal components of the micropulsation field in the frequency range from about 10^{-4} to 1 Hz. In addition, for magnetotelluric application, two horizontal, orthogonal components of the electric field are measured in this same band of frequencies. The sensors for the magnetic field are induction type component magnetometers. The electric field is sensed by a voltage difference measurement between two electrodes. The signals from the sensors are carried by cable to an instrumentation van. Here, the signals pass through various stages of amplification and filtering prior to being

recorded by an FM magnetic tape recorder. A time channel, provided by a precision chronometer, is simultaneously recorded with the signals. This, in brief, contributes a basic magnetotelluric instrumentation system. For the magnetic gradiometer application, a fourth induction coil is located at a remote site. The output of this magnetometer is amplified and filtered and then telemetered to the instrumentation van for recording. The seven channels are recorded continuously for durations up to 17 hours. The data on the magnetic tape, called a run, is returned to the laboratory for analog-to-digital conversion and subsequent analysis.

Two gradiometer sites were made to obtain data for this study. The first site was made furing the summer of 1971 in the vicinity of the Corpus Christi ship channel at Port Aransas, Texas. The second site was made near Manor, Texas in the summer of 1972.

B. Port Aransas

The experiments at Port Aransas were conducted mainly to investigate the capability of the magnetic gradiometer to detect the passage of ships in the Corpus Christi ship channel. However, the series of measurements obtained served several purposes. At that time, the remote sensing unit, including the telemetering system, had not been field tested. It was important to establish the quality of the signal received from the remote site. Another important objective was to acquire actual data from a multicomponent gradiometer for testing the computer programs used for estimation of the geology filter. Although previous experiments had established that the simple differencing type gradiometer could be used effectively as a magnetic anomaly detection system, no multicomponent data was available prior to these measurements. The final objective was to study the spatial coherency of the fields over the baselines employed.

The effect of varying the gradiometer baseline and the remote site distance from the ship channel (detection range) was investigated.

These tests were performed to establish guide lines for possible use of the gradiometer as a detection system. The results can only serve as an indication of what one might encounter at a different site with different perturbation fields. Figure (4-1) shows the configuration of the measurement sites in relation to the ship channel. In these tests only the two horizontal components of the magnetic field variations were measured at the base site. Lack of equipment prevented the measurement of the vertical component, but this posed no real problem for this particular area. Due to the uniform and highly conductive sediments in this region, the vertical component of the field is very small compared to the horizontal components. The two components at the base site were measured perpendicular and parallel to the ship channel. The perpendicular component is designated as H_x and the parallel component is H_y. Three remote sites were used at ranges of 1700, 3400, and 5400 feet from the ship channel. At the remote site, the component of the field that was parallel to the channel was measured and is denoted H_R. The raw null, using the simple differencing scheme, is

$$H_D(t) = H_y(t) - H_R(t). \qquad (4-1)$$

Several recordings which were made during the time that a ship passed through the channel are displayed to demonstrate the ability of the gradiometer to detect at the various ranges. The ships were generally less than 8,000 tons, between 350 and 600 feet long, and had speeds in the range from 8 to 10 knots. When known, the names of the ships are noted in the figures.

The simple differencing scheme, equation (4-1), is used to obtain the null H_D presented in the figures. The component of the field that is perpendicular to the channel, H_x, is displayed; although it is not used for the detection. According to the polarity convention used H_y is opposite in phase to H_R. The difference trace H_D has 5 times the sensitivity of the other traces.

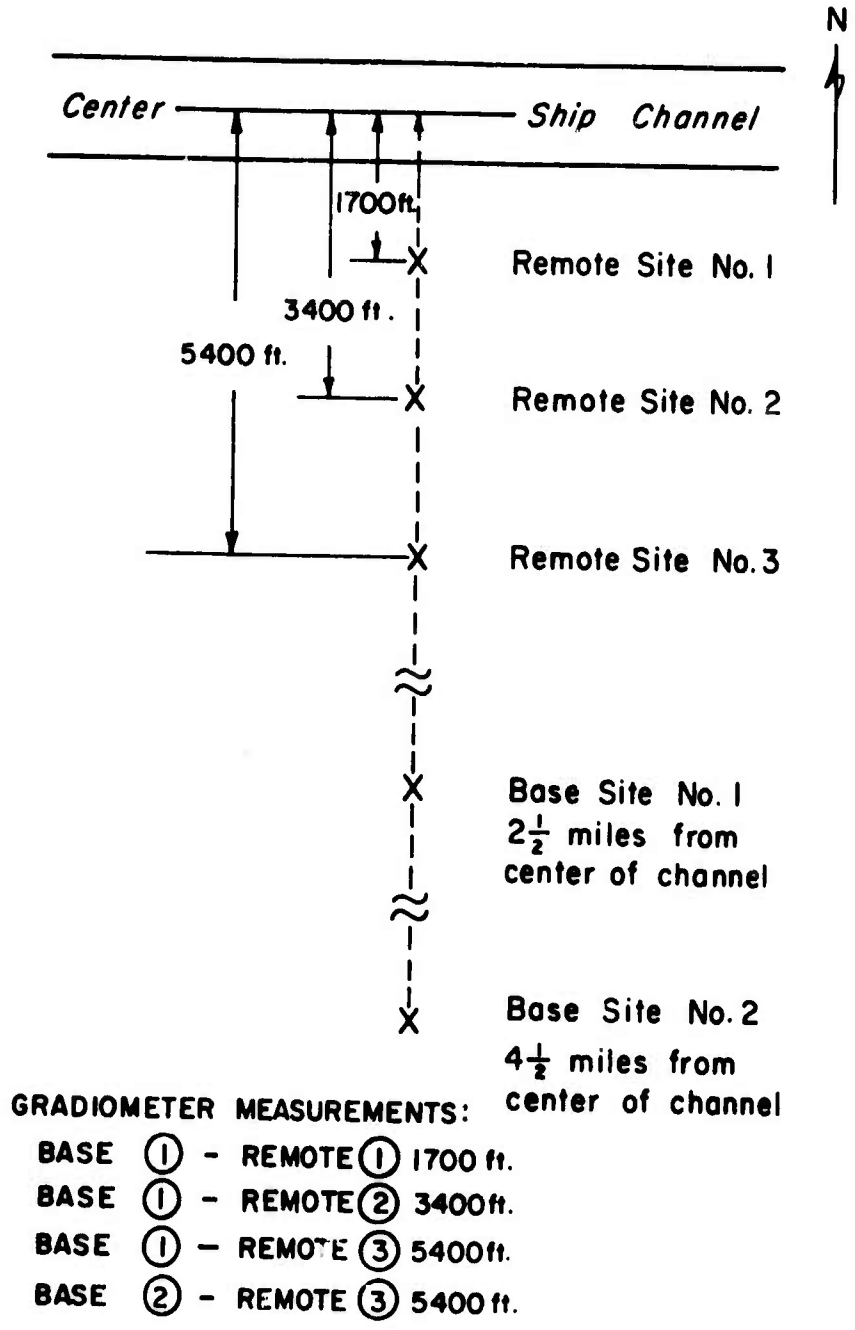

Figure 4-1 Port Aransas Gradiometer Site

For the data displayed in Figure (4-2) the remote site was located at a distance of 1700 feet from the center of the ship channel. A clear signature of the ship appears in the null H_D. At this limited range, the ship passage is also apparent in the remote site trace H_R. However, it is not seen in either H_y or H_x. This figure is typical of the short range data. Detection can usually be made from the H_R trace alone, but signal-to-noise ratio is better in the null H_D. Figure (4-3) is typical of ship passages for the 3400 feet range. The major difference to be noted here is that the ship signature is no longer apparent in the H_R trace as it was in Figure (4-2). At the longer ranges the ship, with its localized field, produces only a small perturbation on the natural micropulsation field. The signature of the ship is detected in the null since in this trace the micropulsation field variations have been cancelled to a large degree. A ship passage for the 5400 feet range is shown in Figure (4-4). This figure is not truly representative of all the data at this range. At times the background noise level in the null is too large to make a sure detection possible.

Without ship passage the residual noise level in the null is on the order of 50 milligamma peak-to-peak at the four mile separation. This value is not to be taken as a measure of spatial incoherency of the source field, since a majority of the noise was traced to the instrumentation. Throughout this series of measurements it appeared that a mechanical chopper in the preamplifier section of the measurement system was causing problems. The redesign of the preamplifier was initiated immediately following the Port Aransas tests and completed early in 1972. Subsequent tests show the system noise level is reduced by approximately a factor of ten over the system used at Port Aransas.

The experiments at Port Aransas were considered a success in several respects. The remote telemetry equipment tested out well and

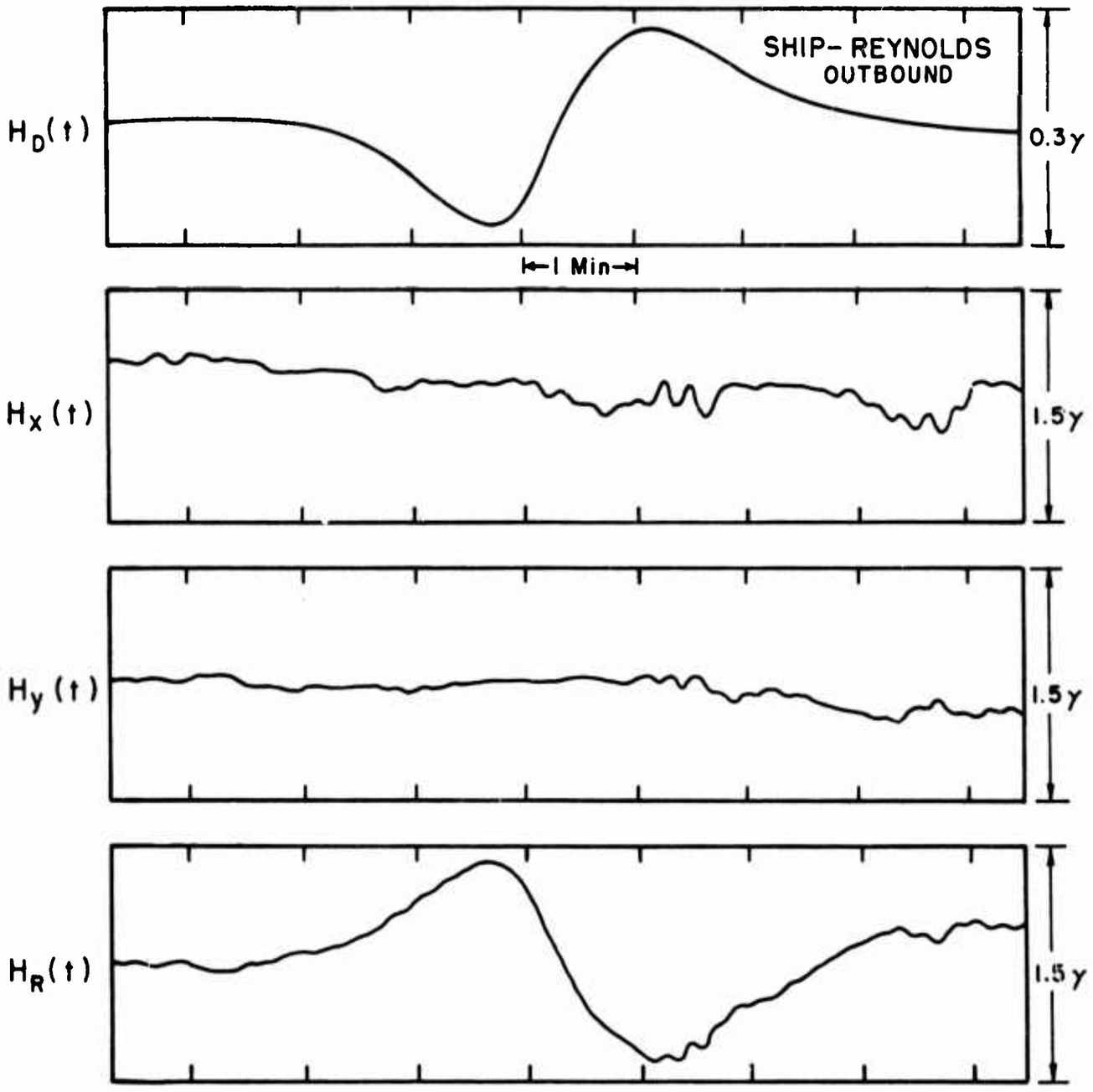

Figure 4-2 Detection of Ship at 1700 Feet

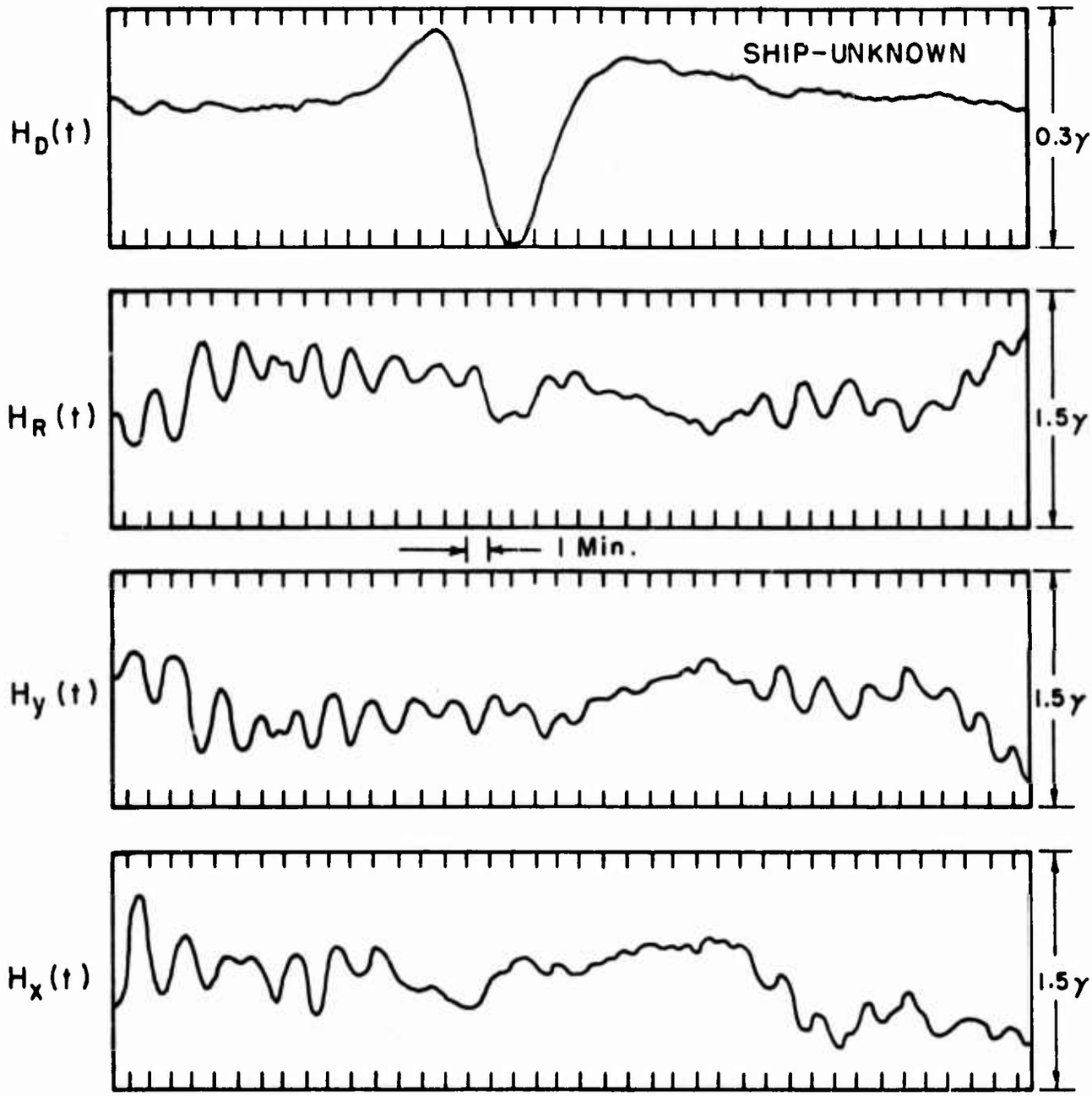

Figure 4-3 Detection of Ship at 3400 Feet

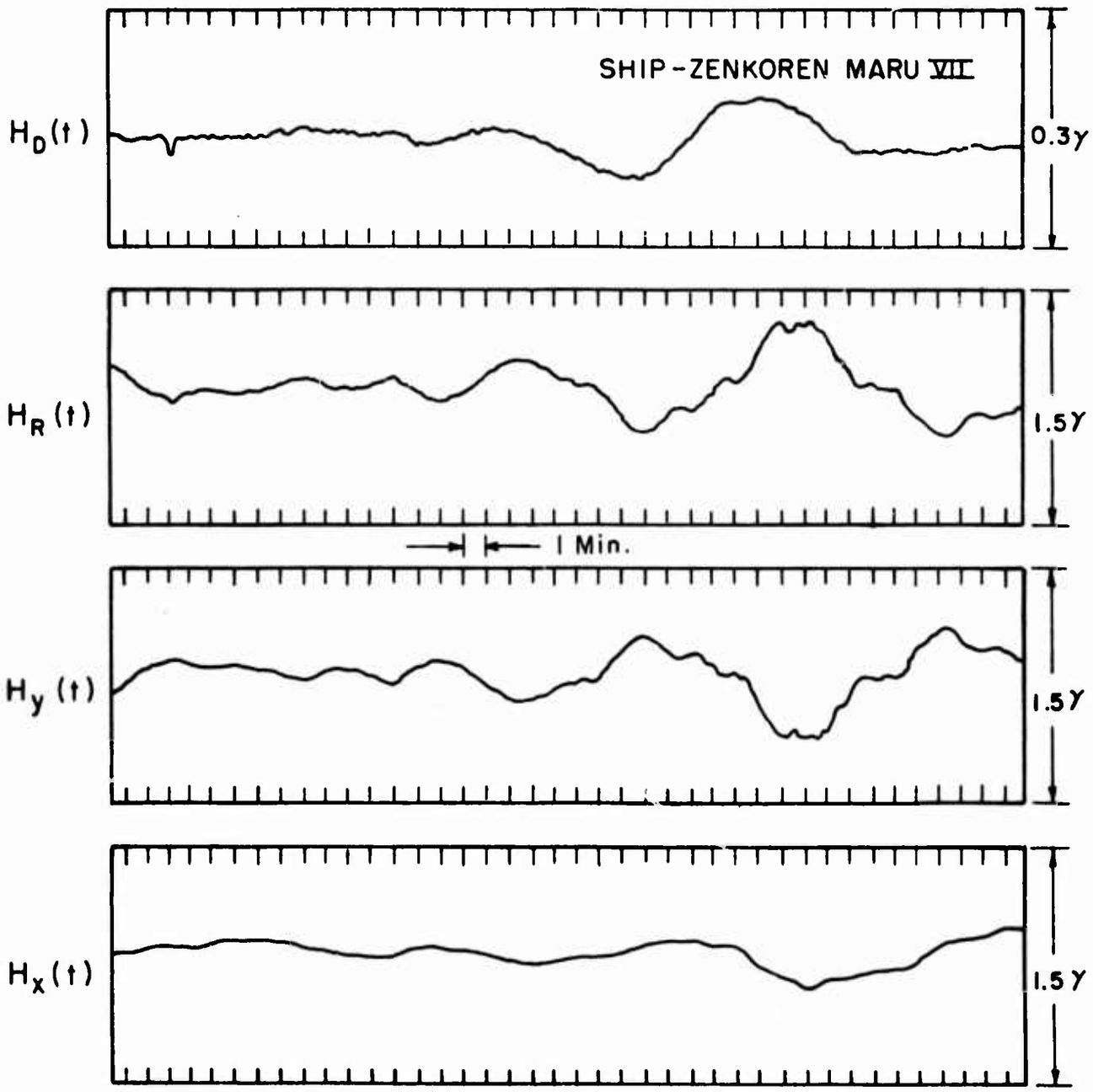

Figure 4-4 Detection of Ship at 5400 Feet

probably most important, the measurements prompted the design of a considerably better measurement system. With the new system, it is estimated that detection of ships in the Corpus Christi channel is possible at ranges extending to two miles.

In addition to these experiments resulting in an improved data system, the following conclusion was reached. The two factors which limit the performance of the detection system are the strength of the perturbation field and the residual noise in the null. The perturbation field is beyond control and any improvements in detection performance must come from consideration of the residual noise in the null.

Aside from system noise, the other possibility of improving detection performance is the utilization of a multicomponent gradiometer system to reduce the effects of the local geology. However, for this particular area the subsurface is so homogeneous that a multicomponent system was not needed.

C. North Manor

A gradiometer site was established in the summer of 1972 near Manor, Texas. From a magnetotelluric survey by Word [19], it is known that this region is geologically more complex than the Texas Gulf Coast. It was suspected that the geology effects would be more pronounced in the measurements from North Manor.

A base site was located at the Thurman Farm north of Manor. Three induction coils were orthogonally oriented by survey. For measurement of the electric field crossed electrode pairs were also laid out. Two remote sites were used for these gradiometer measurements. The configurations are shown in Figure (4-5). In both cases the remote coil was aligned parallel to the Hx coil at the base site. The baseline for Remote Site No. 1 was only 1000 feet. Data from this configuration are used to establish the system noise. Remote Site No. 2 was located 10 miles to the northwest of the base site. Data from this site were analyzed.

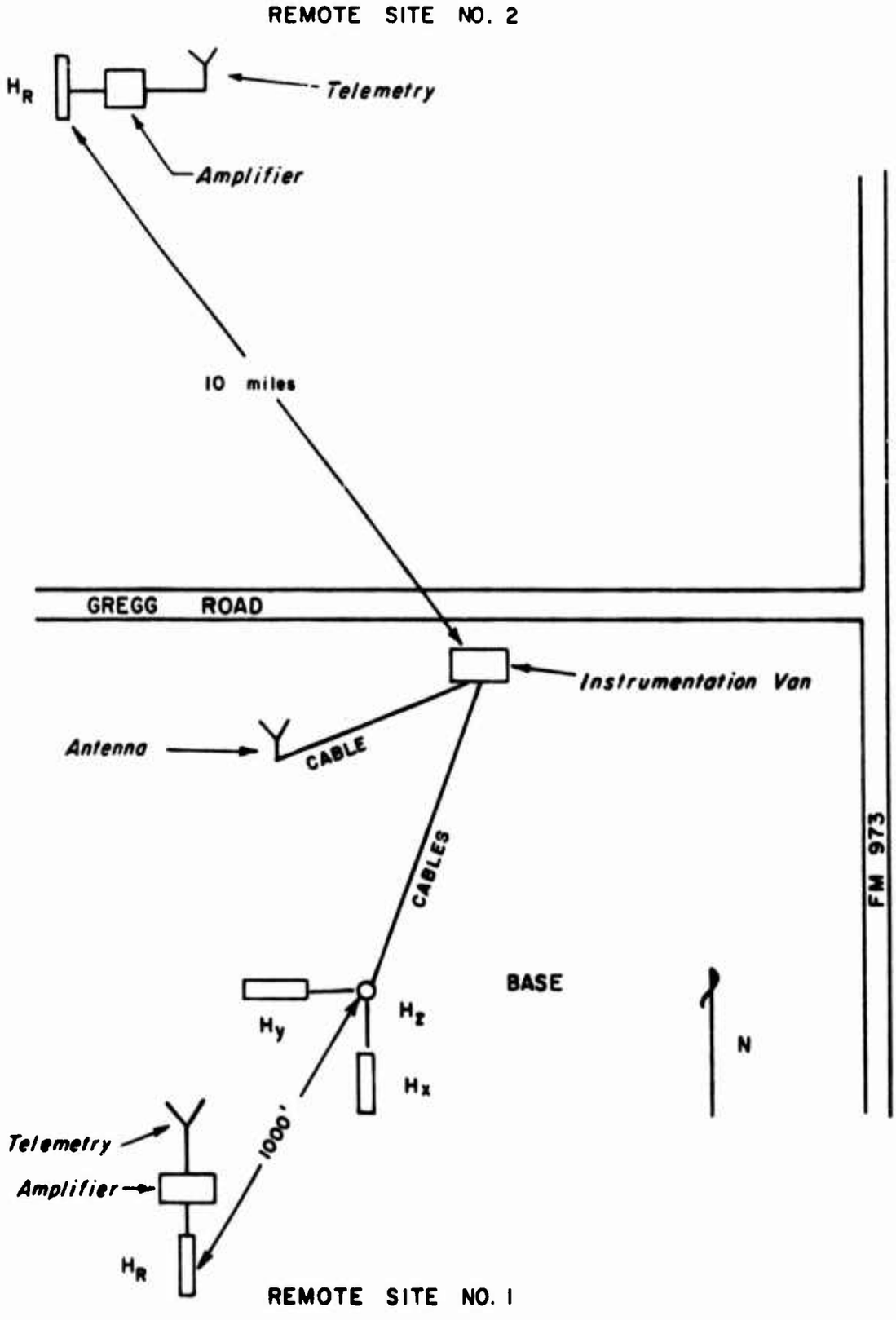

Figure 4-5 North Manor Gradiometer Site

(1) to determine the performance of the geology filter in a more complicated geological situation.

(2) to consider the amount of spatial incoherence of the micropulsation field over the ten mile separation.

(3) to judge the ability of the gradiometer system to detect the passage of automobiles.

In addition, the data from the electric field measurements are also used. It will be shown later how it is possible to use a standard magnetotelluric site as a detection system.

1. Remote Site No. 1

The remote coil for these tests was installed with considerable care. The field crew attempted to align the remote coil exactly parallel to the Hx coil at the base site. Over the baseline of 1000 feet, it is assumed that spatial incoherency of the source field and the geology effects are negligible. Provided that the two coils are in exact alignment, the power in the raw null between the two parallel coils is due to

(a) measurement system noise,

(b) telemetry system noise,

(c) slightly different filter response curves for the individual channels.

A typical section of data acquired from Remote Site No. 1 is shown in Figure (4-6). Except for the polarity convention, the remote site trace H_R appears identical to its parallel component H_x at the base site. The differences in the two traces are shown in the raw null H_D which has a gain factor of ten. Inspection of the raw null shows that it retains some correlation with H_R. This indicates a slight gain difference on the order of 5% between the H_x and H_R channels. The gain difference is of no real consequence, since its removal is a simple correction. The raw

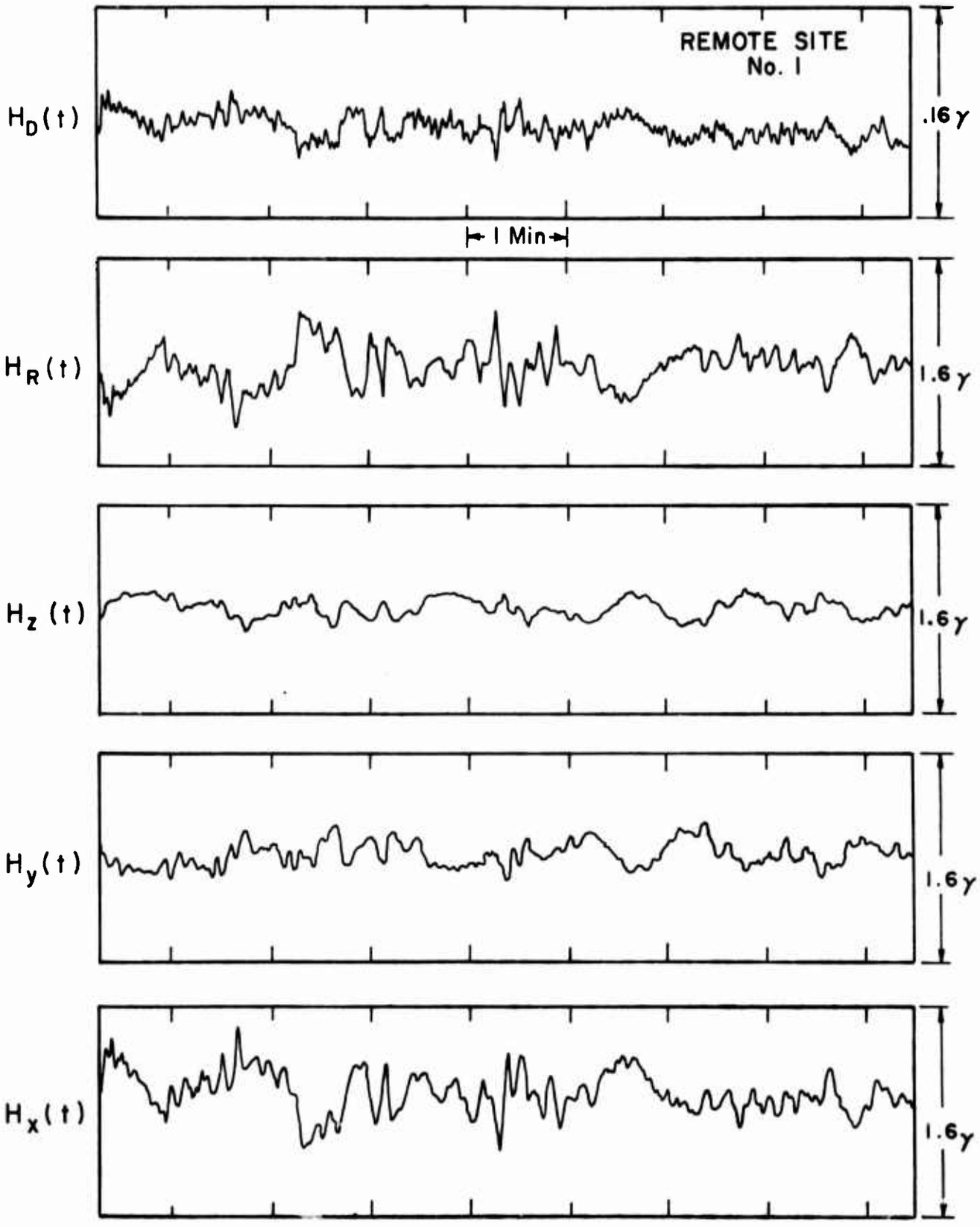

Figure 4-6 Run No. 15. Remote Site No. 1

null is also correlated to an extent with both H_y and H_z. It is possible that the assumption of negligible geology effects and spatial coherency is invalid. It is more likely, however, that the two sensors H_x and H_R are not exactly parallel. As previously discussed, misalignment is an important consideration. It may produce an apparent incoherency in the measured fields which is indistinguishable from the effects of inhomogeneous geology.

Since the geology filter will account for misalignment as well as for geology effects, the filtered null is used here as a measure of the system noise. The data from Remote Site No. 1 were used to estimate the geology filter in accordance with the frequency domain approach presented in Section III. The filtered null $H_F(f)$ is obtained using Equation (2-1). The sample variance of the filtered null is given by

$$\sigma_F^2 = \frac{1}{2(N-1)} \sum_{t=0}^{N-2} [h_F(t+1) - h_F(t)]^2 \qquad (4-4)$$

where $h_F(t)$ is the inverse Fourier transform of $H_F(f)$ and $\bar{h}_F$ is the sample mean

$$h_F = \frac{1}{N} \sum_{t=0}^{N-1} h_F(t). \qquad (4-5)$$

For the detection system, the objective is to cancel the micropulsation field variations between the two measuring sites. A performance measure for the amount of cancellation is the ratio of the null variance to the variance of the remote site trace. The performance figure is defined as

$$P_F = 10 \log_{10} \frac{\sigma_F^2}{\sigma_R^2} \qquad (4-6)$$

and is presented in decibels.

Two runs using this remote site were judged suitable for analysis. After designing and applying the geology filter for each run, the performance figures of -31.6 dB and -37.4 dB were obtained. This indicates that the power in the filtered null is between 0.02 and 0.1% of the power contained in the remote site trace. The lower figure represents excellent cancellation, on the order of instrumentation noise.

2. Remote Site No. 2

After manual editing of the data, four runs from Remote Site No. 2 were considered usable for analysis. This data is used to determine the amount of micropulsation field cancellation which can be expected over a ten mile baseline. The data is also analyzed to determine the ability of the gradiometer to detect the passage of automobiles.

Although it may be misleading to consider simple coherency relationships between parallel components of two vector fields, a coherency analysis was performed. Typical auto power spectra for this data are shown in Figure (4-7). The frequency content of the two parallel coils is almost identical. The sample coherence between the two parallel coils is defined as

$$\gamma^2 = \frac{|\overline{H_x H_R^*}|^2}{(\overline{H_x H_x^*})(\overline{H_R H_R^*})}$$

where $\overline{H_x H_R^*}$ is the average cross power spectrum at a given frequency. The terms in the denominator are the two auto power spectra at this frequency.

For this data, the sample coherence is consistently above 0.98 in the frequency range from 2.5×10^{-4} Hz to 2.0×10^{-2} Hz. This indicates that not only is there very little spatial incoherency in the source wave over the ten mile separation, but the geology effects are also small.

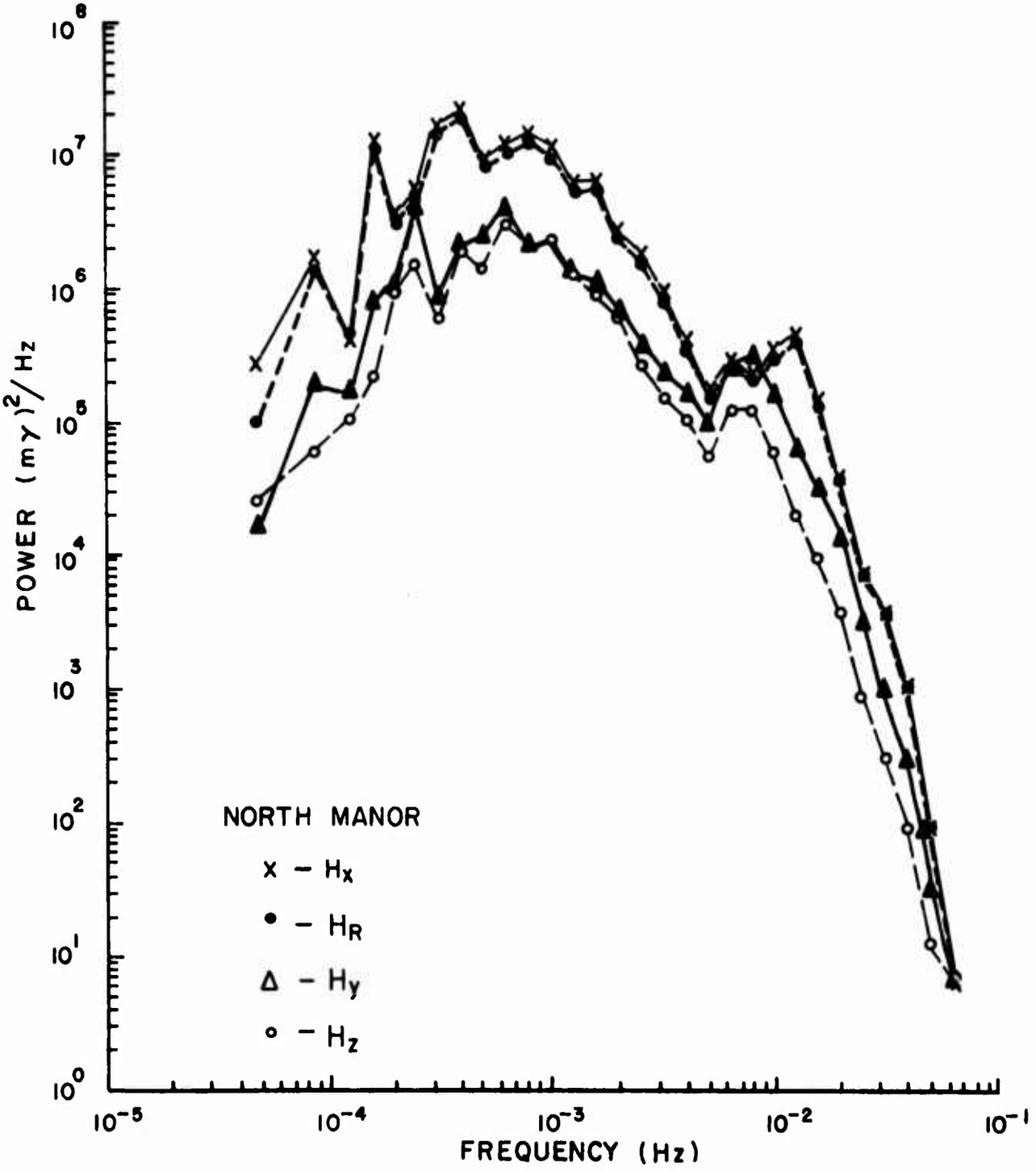

Figure 4-7 Typical Auto Power Spectra. Remote Site No. 2

Geology filters were estimated for each of the four runs using the frequency domain approach. Each of the four filters were then applied to the data from which they were designed. The results are presented in Table (4-1). The sample variances of the remote site trace, the raw null, and the filtered null are each given in units of milli-gamma squared. The performance figures of the raw null and the filtered null are presented in decibels.

Table (4-1) demonstrates the utility of the geology filter, especially for detection applications. The performance figure for the filtered null is approximately 14 dB better than that of the raw null. The reduction of power in the filtered null amounts to an improvement of the signal-to-noise-ratio when an anomaly is present. For a given perturbation field strength this is also equivalent to an increase in the detection range. For perturbation signals that obey an inverse cube law, this represents an increase in detection range by a factor of 1.7.

It is difficult to say whether the improvement in the cancellation of the micropulsation field after application of the geology filter is entirely due to the removal of the geology effects. It is likely that part of the improvement comes from correction for gain differences, coil misalignment, and filter mismatch; since the geology filter corrects for these factors as well as accounting for inhomogeneous geology. For the detection system, correction for these factors is a very nice feature of the geology filter. In a tactical situation it may be impossible to survey in the coils. With the use of the geology filter, it is really not necessary.

Table (4-1) also yields useful information about the spatial coherency of the source wave over short distances. The average performance figure for the filtered null over the ten mile baseline is on the order of -34 dB. On the average the filtered null contains only 0.04% of the power contained in the remote site trace. The worst

Run No.	σ_R^2	σ_D^2	P_D	σ_F^2	P_F
1	7.7×10^4	4.4×10^2	-22.4 dB	17.4	-36.4 dB
8	1.0×10^5	1.2×10^3	-19.2 dB	40.0	-34.0 dB
11	7.0×10^4	9.6×10^2	-18.6 dB	64.1	-30.4 dB
12	1.2×10^5	1.1×10^3	-20.4 dB	31.6	-35.8 dB

TABLE 4-1

Filter Performance

Run No.	Filtered By	σ_F^2	P_F
8	11	88.6	-30.6
8	12	84.2	-30.8
11	8	105.6	-28.2
11	12	123.4	-27.4
12	8	67.2	-32.5
12	11	104.0	-30.6

TABLE 4-2

Stability of Geology Filter

case is Run No. 11 which has a performance figure of -30.4 dB. In order to compare the average performance figure for the ten mile baseline to the system noise performance figure obtained from Remote Site No. 1, one must consider the reliability of the estimates. A variance ratio test outlined in the appendix indicates that the confidence interval at the 90% level is ± 3.4 dB. Since the confidence interval for the average performance figure for the ten mile baseline and the system noise performance figure are overlapping, it is concluded that the differences are not statistically significant. For this analysis, the system noise, although extremely small, is too great to allow making any concrete statements about spatial incoherency over a ten mile baseline.

For application of the magnetic gradiometer as a detection system, an important consideration is whether the geology filter improves the signal-to-noise ratio enough to warrant its use. In some cases, such as for this Port Aransas area, the simple differencing scheme is adequate. However, for the North Manor site, Run No. 1 will be used to demonstrate that the geology filter provides a worthwhile improvement in the signal-to-noise ratio. Run No. 1 was selected for this analysis because it was known when several automobiles passed along Gregg Road. Gregg Road is the farm road shown in Figure (4-5). The center of the three orthogonally oriented coils at the base site is 500 feet from the centerline of the road. A section of the data from this run is presented in Figure (4-8). Note that the H_x and H_R traces again have reversed polarities. Hence the raw null H_D is obtained by adding H_x and H_R. The filtered null $H_F(t)$ is the inverse Fourier transform of $H_F(f)$ obtained from Equation (2-1). Both H_D and H_F have been scaled up by a factor of ten over the other traces. Time ticks are given each minute in the figure.

A pickup truck passed along Gregg Road approximately 12 minutes from the beginning of this section of data. The signature of the truck is clear in both the raw null and the filtered null traces.

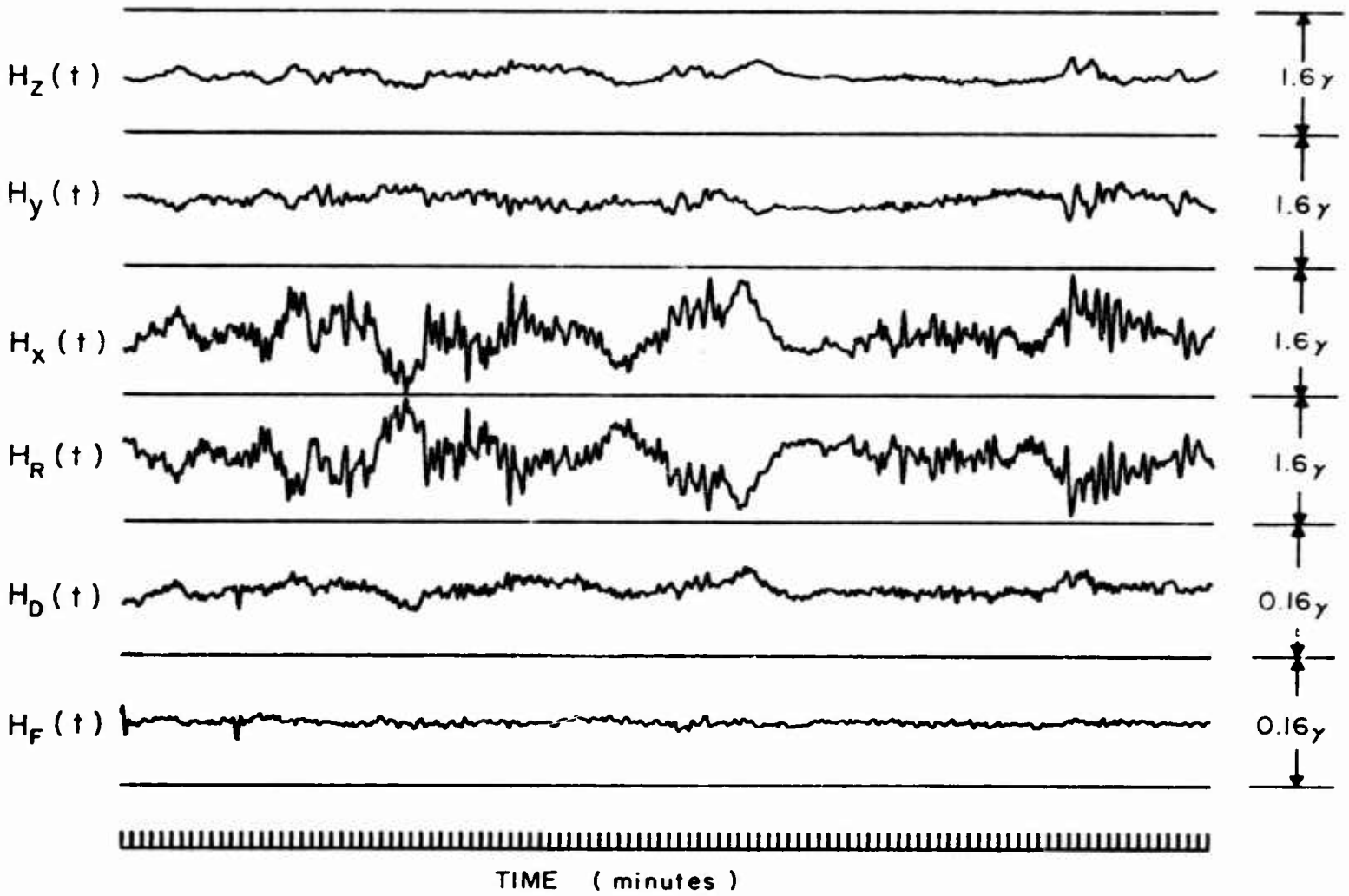

Figure 4-8 First Section of Data From Gradiometer Run 6-27-72-1

However, the improvement in signal-to-noise ratio in the filtered null should be apparent to the eye. The signal-to-noise ratio is defined here as

$$SNR = 20 \log_{10} \frac{P}{\sigma} \qquad (4\text{-}7)$$

where P is the absolute value of the peak excursion of the anomaly signal and σ is the rms power of the noise when no signal is present. The SNR for the raw null is 9.5 dB. The filtered null has a SNR of 16.0 dB, this is an improvement of 6.5 dB in signal-to-noise ratio. It is particularly impressive when one compares this to the signal-to-noise ratio for a single component, say the H_x trace. The SNR for the H_x trace is approximately -20 dB. The filtered null provides an improvement of 36 dB.

Another section of data from Run No. 1 is presented in Figure (4-9). In this section there are two apparent signatures. One occurs about the middle of the data and the other is approximately 22 minutes before the end of this data. The use of the geology filter improves the SNR to a noticable degree. Quantitatively, the improvement is 5.0 dB for the first anomaly and 6.4 dB for the second.

Comparison of the automobile signatures in these figures to the ship signatures shown previously shows that the time durations of the automobile signals are much shorter than the ship signals. This is due primarily to the differences in range and velocity. In actual operation of the detection system, a priori knowledge of the range and velocity of a target would be unknown. Hence, frequency content or time signature of the target would be unknown. It has been a prime consideration in this study to keep the signal processing broadband in order to detect a target whose frequency content may be anywhere in the bandwidth of the measuring system. This is not intended to preclude the possibility of departing from broadband processing. Reducing the bandwidth would be

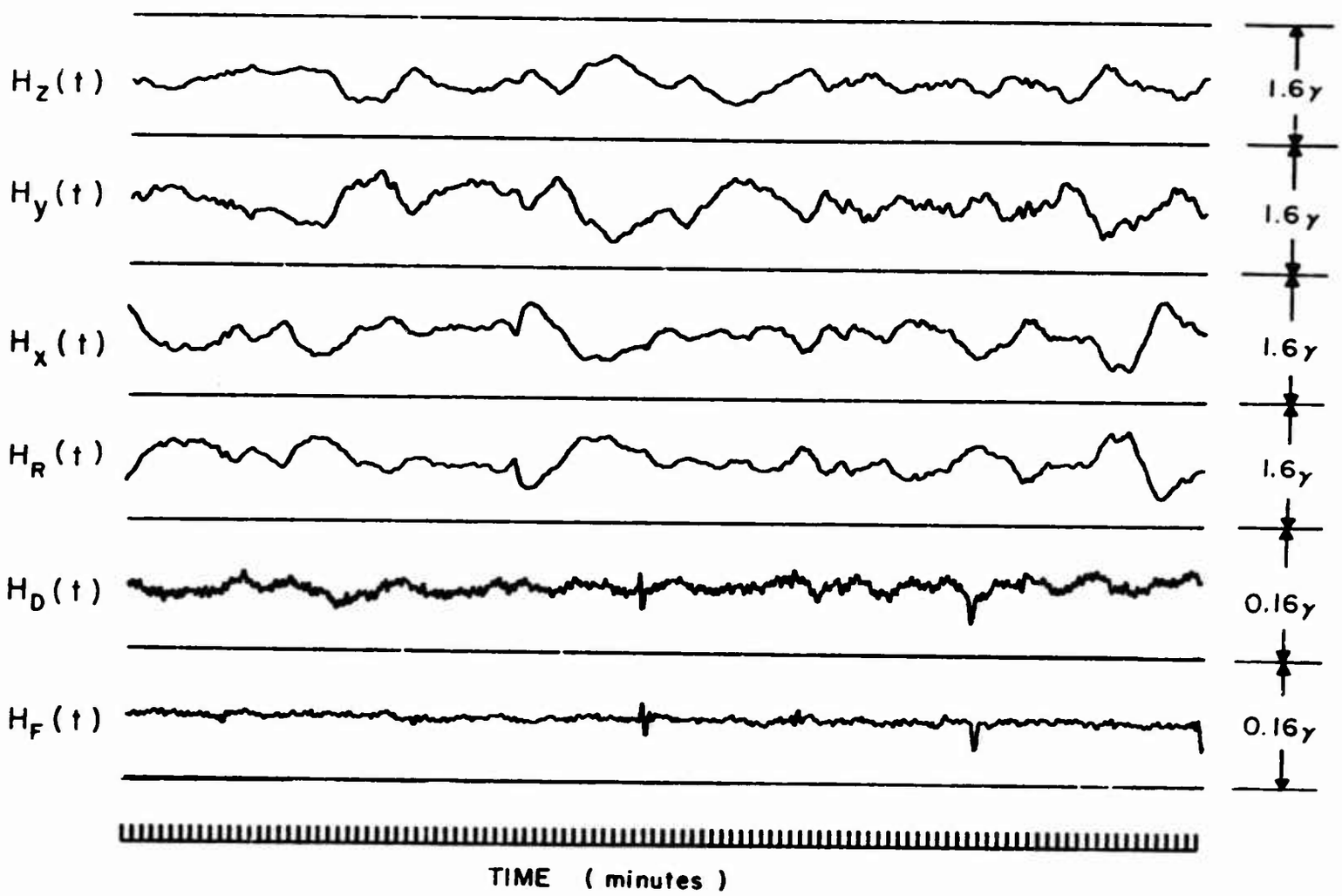

Figure 4-9 Last Section of Data From Gradiometer Run 6-27-72-1

desirable for applications where bounds have been established on the target signatures. Note that in the raw nulls shown in Figures (4-8) and (4-9) the signal-to-noise ratios could be improved considerably by removing the low frequency ripple through the use of a suitable high pass filter. Unfortunately for real time operation, this might very well result in a system that would reject targets that passed at a much slower speed.

If the magnetic gradiometer is to be used as a detection system, another important consideration is whether or not the geology filters are time varying. From the physics of the situation, there is no reason to expect the filters to vary with time unless the subsurface geology varies. The results given in Table (4-1) are obtained using geology filters operating on the same data from which they were designed. An aposteriori analysis is probably not desireable for a detection system. It is more likely that the filters will be designed and then expected to perform on fresh data so that detection can be made in real time. An analysis of the time variability of the geology filters is made by taking the filter designed from a particular run and filtering the data from another run. The data from Run No. 1 are not used in this analysis due to a difference in equipment between it and the other runs. All possible combinations of filter and data are used for the remaining three runs. The results, in terms of the filtered null variance and the performance figure, are given in Table (4-2).

As expected, the performance figures for the filtered null in Table (4-2) are not quite as good as the performance figures for the filtered null in Table (4-1). On the average there is about 4 dB degradation due to using fresh data. This represents excellent time stability of the filter. Comparing the performance figures in Table (4-2) to the performance figure for the raw null in Table (4-1), it is seen that the geology filter provides approximately 10 dB improvement in the cancellation of the micropulsation field.

Another interpretation of Table (4-2) is possible. It is unlikely that the subsurface geology at the measuring site in North Manor changed considerably during the time of these measurements. If the geology filters are time invariant, then the results presented in Table (4-2) are a measure of the reliability in the estimation of the geology filter. From either viewpoint, it appears that the method of estimation in the frequency domain, using constant Q averaging, is an acceptable approach.

3. Base Site

In this section it will be shown how the magnetotelluric measurement system itself may be used as a detection system. The remote site is not a necessity for this application. Experimentalists in the magnetotelluric area are aware that after a run has been started, it is not wise to allow traffic in the vicinity of the sensors. A passing truck can cause a considerable perturbation in the output of the magnetic field sensors. However, the effect is usually small in the output of the electric field sensors. Since the electric field is generated by the time varying magnetic field over a very large area, the localized field of an anomaly makes little difference in the output the electrode pairs.

In magnetotelluric analysis the tensor impedance is written

$$\begin{bmatrix} E_x \\ E_y \end{bmatrix} = \begin{bmatrix} Z_{xx} & Z_{xy} \\ Z_{yx} & Z_{yy} \end{bmatrix} \begin{bmatrix} H_x \\ H_y \end{bmatrix}$$

where the dependence on frequency is suppressed. Estimation of the elements of the tensor impedance is made in much the same manner as the frequency domain approach for the geology filter. After estimation, either of the above two equations may be used to detect the passage of a magnetic anomaly. An error signal is defined

$$E_F(f) = E_x(f) - Z_{xx}(f)\, H_x(f) - Z_{xy}(f)\, H_y(f)$$

or

$$E_F(f) = E_y(f) - Z_{yx}(f)\, H_x(f) - Z_{yy}(f)\, H_y(f).$$

In the absence of an anomaly signal $E_F(f)$ is considered as an error trace in relating a component of the electric field to the two horizontal components of the magnetic field. When an anomaly signal is present the measured micropulsation fields contain a term which was not accounted for in the estimation of the tensor. Thus the anomaly signal appears in the null trace $E_F(f)$.

Since the anomaly signal also appears in the vertical component of the magnetic field, it is possible to again use a four channel system by defining the null as

$$E_F(f) = E_x(f) - A(f)\, H_x(f) - B(f)\, H_y(f) - C(f)\, H_z(f).$$

A similar expression may be written for the other component of the electric field. There is no difference in form for this null and the one defined for the magnetic gradiometer. The information from the remote site trace H_R is replaced by the electric field information at the base site.

Estimation and application of this filter may be accomplished using the methods presented and this was done for Run No. 1. The performance figure for this filter is defined

$$P_E = 10 \log_{10} \frac{\sigma_F^2}{\sigma_E^2}$$

where σ_F^2 is the sample variance of the filtered null and σ_E^2 is the sample variance of the electric field component used.

For this run the performance figure is -23.8 dB. It is not completely understood why this method does not compare more favorably with the magnetic gradiometer. Perhaps the electric fields are just naturally more disturbed in this area than are the magnetic fields. Channeled currents are also a possibility. In any case, the performance figure here represents a usuable amount of cancellation. This method especially warrants further consideration for the detection application if one is prevented, in a tactical situation, from using a remote site.

V. CONCLUSIONS AND RECOMMENDATIONS

This study has resulted in a considerably improved measurement system for the magnetic gradiometer. The noise figure for the measurement system with the sensors operating at ambient temperature is approximately 5 dB at present. The noise in the measurement system cannot be reduced below the thermal noise level of the induction coil sensors. This noise is only 5 dB below the system noise and any improvements of this size would permit only a negligible increase in detection range. The recent development of cryogenic magnetometers using superconducting elements to sense component fields offers the possibility of significant noise level reductions. Increases in detection ranges appear possible, but are accompanied with the attendant operational problems of the cryogenic system. The Electrical Geophysics Research Laboratory has cryogenic systems under consideration, but as yet no gradiometer experiments have been conducted.

In addition to an improved data system, it has been shown that the detection capabilities of the magnetic gradiometer may be improved through the use of the geology filter. The improvement that may be obtained depends upon the complexity of the loacl geology. There are areas, such as the Texas Gulf Coast, where the subsurface is very homogeneous. For these types of

gradiometer sites, the geology does not warrant using a filter. However, part of the improvement in detection performance may be attributed to the ability of the geology filter to correct for coil misalignment and differences in measurement system response. One might wish to use the geology filter for these corrections. In any case it is a straight forward and inexpensive process to estimate the geology filter and the available improvement.

Aside from its use as a detection system, the magnetic gradiometer provides an excellent tool for the study of the micropulsation source field. In the absence of a target anomaly the filtered null is indicative of spatial incoherency in the incident wave. This question is of considerable importance to those interested in magnetotellurics. There is considerable controversey over the spatial uniformity of the source field and perhaps one of the reasons is that the geology differences between the measuring sites have not been considered in enough detail. The gradiometer presents a technique which accounts for the perturbing effects of the geology.

The Electrical Geophysics Laboratory has recently been engaged in the design of an audio frequency magnetotelluric system. This system should become operational in the very near future. In addition to the above recommendations, it is suggested that the frequency range of the magnetic gradiometer may be extended into the audio region. A gradiometer, at these higher frequencies, should be able to detect smaller objects.

BIBLIOGRAPHY

1 Bendat, J. S., and A. G. Piersol , 1966: Measurement and Analysis of Random Data, John Wiley and Sons, Inc., New York, N.Y.

2 Blackman, R. B., and J. W. Tukey, 1958: The Measurement of Power Spectra, Dover Publications, New York, N.Y.

3 Bostick, F. X., Jr., 1968: "Magnetotelluric and Telluric Instrumentation," paper presented at the symposium on Application of Natural Electromagnetic Fields in Petroleum and Mining Exploration, College of Engineering, University of California, Berkeley.

4 Cagniard, Louis, 1953: "Basic Theory of the Magneto-telluric Method of Geophysical Prospecting," Geophysics. XVIII, No. 3, pp. 605-635.

5 Hermance, J. F., and W. R. Peltier, 1970: "Magnetotelluric Fields of a Line Current," Jour. Geophys. Res., Vol. 75, No. 17, pp. 3351-3356.

6 Hopkins, George H., Jr., 1965: "Instrumentation for Geofield Measurements," Electrical Engineering Research Laboratory, The University of Texas, Nonr Report No. 138.

7 Madden, T., 1964: "Spectral, Cross-Spectral, and Bispectral Analysis of Low Frequency Electromagnetic Data," Natural Electromagnetic Phenomena Below 30 kc/s, Plenum Press, New York, N.Y.

8 Madden, T., and P. Nelson, 1964: "A Defense of Cagniard's Magnetotelluric Method," ONR Project NR-371-401, Geophysics Lab., M.I.T.

9 Pennington, Ralph H., 1965: Introductory Computer Methods and Numerical Analysis, MacMillan, New York, N.Y.

10 Price, A. T., 1962: "The Theory of Magnetotelluric Methods When the Source Field is Considered," Jour. Geophys. Res., Vol. 67, No. 5, pp. 1907-1918.

11 Robinson, E. A., 1967: Multichannel Time Series Analysis with Digital Computer Programs, Holden-Day, Inc., San Francisco, California.

12 Sims, W. E., 1969: Methods of Magnetotelluric Analysis, Ph.D. Dissertation, The University of Texas at Austin.

13 Swift, Charles M., 1967: A Magnetotelluric Investigation of an Electrical Conductivity Analog in the Southwestern United States, Ph.D. Dissertation, M.I.T.

14 Tammemagi, Hans Y., 1972: A Magnetotelluric Study in South Eastern Australia, Ph.D. Dissertation, Australian National University.

15 Wait, James R., 1954: "On the Relation Between Telluric Currents and the Earth's Magnetic Field," Geophysics, XIX, No. 2, pp. 281-289.

16 Wiggins, R. A., and E. A. Robinson, 1965: "Recursive Solution to the Multichannel Filtering Problem," Jour. Geophys. Res., Vol. 70, pp. 1885-1891.

17 Word, Darrell R., 1970: An Investigation of the Magnetotelluric Tensor Impedance Method, Ph.D. Dissertation, The University of Texas at Austin.

18 Zelwer, R., and H. F. Morrison, 1971: "Spatial Characteristics of Magnetotelluric Fields," paper presented at Forty-First Annual International SEG Meeting.

APPENDIX

The performance measure used in this study is the ratio of two sample variances. It is assumed that the two variances σ_F^2 and σ_R^2 are independent random variables. Let σ_F^2 have a chi-square distribution with n_1 degrees of freedom and σ_R^2 have a chi-square distribution with n_2 degrees of freedom. The random variable F_{n_1,n_2} is defined as

$$F_{n_1,n_2} = \frac{\sigma_F^2/n_1}{\sigma_R^2/n_2}$$

This random variable is the F variable with n_1 and n_2 degrees of freedom. The probability density function for F_{n_1,n_2} is

$$p(F) = \frac{\Gamma[(n_1 + n_2)/2]\ (n_1/n_2)^{n_1/2}\ F^{(n_1/2) - 1}}{\Gamma(n_1/2)\ \Gamma(n_2/2)\ [1 + (n_1F/n_2)]^{(n_1 + n_2)/2}}$$

where $\Gamma(n/2)$ is the gamma function. Percentage points have been tabulated for the F or variance ratio distribution. Limited tables may be found in Bendat and Piersol [1].

If the true value of the performance measure is P_F, the confidence interval at the $(1 - \alpha)$ confidence level is obtained from

$$\left[\frac{\sigma_F^2}{\sigma_R^2} F_{n_1,n_2} - \alpha/2 < P_F \leq \frac{\sigma_F^2}{\sigma_R^2} F_{n_1,n_2,\alpha/2} \right]$$

Inspection of the power spectra presented in Figure (5-7) shows that the data used in this analysis are not white. For non-white data, Blackman and Tukey [2] present a method for obtaining an approximation to the equivalent number of degrees of freedom. The approximation is

$$n = \frac{2(p_o + p_1 + p_2 + \ldots)^2}{p_o^2 + p_1^2 + p_2^2 + \ldots}$$

where each of the p_o, p_1, p_2,... is the power at a given frequency in the estimate of the spectrum. Using this approximation, it is found that the equivalent number of degrees of freedom is only 18. This is a considerable reduction from the 8192 degrees of freedom that might be used for the raw spectrum.

Using this equivalent degrees of freedom, $n_1 = n_2 = 18$. The confidence interval at the 90% level, $\alpha = 0.10$, is

$$\left[\frac{\sigma_F^2}{\sigma_R^2} 1/F_{18,18,0.03} < P_F \leq \frac{\sigma_F^2}{\sigma_R^2} F_{18,18,0.05} \right]$$

From Table 4.10(a) in Bendat and Piersol, it is found that $F_{18,18,0.05} = 2.22$. Thus

$$\left[\frac{\sigma_F^2}{\sigma_R^2} (1/2.22) < P_F \leq \frac{\sigma_F^2}{\sigma_R^2} (2.22) \right]$$

with a confidence of 90%. With these simplifying assumptions about the independence and the distributions of the sample variances, the 90% confidence interval for the performance figures is $\pm$ 3.4 dB.

The method of establishing the confidence interval is left open to question. Since the micropulsation data are non-stationary, there is an additional degree of uncertainty in the performance figure. The confidence intervals are thus presented as a point of reference; at times they could be much better or much worse than the values given. A more valid approach would be to establish experimental confidence levels. This would require a large number of experiments which are, unfortunately, unavailable at the present time. However, on the basis of the data at hand, the values given here are not considered totally out of line.